Eur. Phys. J. B **3**, 109–117 (1998)

THE EUROPEAN PHYSICAL JOURNAL B

Inelastic neutron scattering from H_2 on vapour deposited CO_2

A. Knipp[1,a], W. Langel[1,b], H. Mutka[2], and E. Knözinger[1,c]

[1] Fachbereich Chemie der Universität Siegen, 57068 Siegen, Germany
[2] Institut Laue-Langevin, BP 156, 38042 Grenoble Cedex 9, France

Received: 15 October 1996 / Revised: 25 August 1997 / Accepted: 24 October 1997

Abstract. Inelastic neutron scattering spectra at 17 meV and 68 meV incident energies of molecular hydrogen adsorbed on vapour deposited substrates of pure CO_2, 90:10 and 50:50 CO_2:Kr are reported. The ortho-para transition is shifted from 14.7 meV in the free H_2-molecule to 9.4 meV in a presumably commensurate ortho-H_2 monolayer on the CO_2 surface. The quadrupole-quadrupole interaction of ortho-H_2 molecules with the CO_2 substrate results in a strongly anisotropic potential. In addition to rotations the dynamics of this layer comprise a local Einstein mode and phonons in resonance with the substrate, giving rise to intense multiphonon transitions. Quasielastic scattering on warmer samples is assigned to a liquidlike adsorption layer, in which the H_2 rotations are strongly perturbed.

PACS. 29.30.Hs Neutron spectroscopy – 68.35.Ja Surface and interface dynamics and vibrations – 33.15.Fm Bond strengths, dissociation energies

1 Introduction

In many cases structure, dynamics and morphology of vapour-deposited solids strongly differ from those of the corresponding equilibrium phases. The fast condensation at temperatures far below the respective melting points leads to a high nucleation rate and, consequently, to very fine grains. Such phases are metastable and sinter into more stable modifications at higher temperatures thereby reducing their high surface energies. Among the systems which were studied under this aspect are ice [1] and carbon dioxide [2] since their condensation processes in space may resemble vapour deposition [3]. In addition to that the molecular dynamics of carbon dioxide are of fundamental interest for the supercritical fluid extraction as applied in large scale for various purposes [4].

By X-ray diffraction we demonstrated that solid carbon dioxide does not exhibit such a substantial degree of disorder after gas-phase deposition [2,5] as was observed for ice or solid rare gases under similar conditions [6,7]. The Bragg reflections of CO_2 were broadened, however, with respect to those of the sample support, and diffuse intensity between the reflections was observed. These diffractograms were fitted by patterns as calculated for a logarithmic normal distribution of the CO_2 grain size with an average diameter of 3 nm [8]. According to molecular dynamics simulations even in such small units the bulk crystalline structure is maintained and surface relaxation is insignificant [8,10]. The intermolecular interaction of carbon dioxide may well be described by classical pair potentials [5]. The dominant contribution is due to its strong quadrupole moment (-3.17 a.u. [9]), which induces orientational order in the solid.

CO_2 and Kr do not form thermodynamically stable solid mixtures, even though the structures and lattice constants of the pure solids are very similar to each other [5]. By vapour deposition solid mixtures with severely perturbed structures were obtained. In the intermediate concentration range (30−70 mol% of Kr) they are fully amorphous. We attributed this disorder to a loss of the coherence of the molecular orientations induced by the dilution with Kr atoms.

The small grain size of vapour deposited CO_2 results in a high specific surface area [8,11–14]. Significant amounts of hydrogen of up to 15 mol% of the substrate are adsorbed, and the system was proposed as a hydrogen pump [14]. A complication is that o-H_2 has a significant quadrupole moment (0.485 a.u.) whereas the quadrupole moment of p-H_2 is zero [15]. The sorption capacity seems to depend very sensitively on the surface structure and is considerably reduced by the addition of small amounts of krypton to the matrix [8]. This observation was explained by a simple model [16] providing regular sites with 4-9 next neighbours depending on the crystallographic type of the surface. By codepositing the mixtures surface sites with both CO_2 and Kr next neighbours are obtained. The number of sites with only CO_2 next neighbours is strongly decreasing with increasing molar ratio of Kr. By assuming

[a] *Present address*: Edwards Hochvakuum GmbH, 85551 Kirchheim/Munich, Germany
[b] e-mail: `langel@chem735.chemie.uni-greifswald.de`
[c] *Present address*: Institut für Physikalische Chemie der Technischen Universität Wien, Getreidemarkt 9, 1060 Wien, Austria

that each site which contains at least one Kr next neighbour to the adsorbed particle is already inactive for H_2 adsorption the observed low hydrogen uptake in CO_2:Kr substrates was modelled. Another possibility is, that krypton which has a much higher vacuum pressure than carbon dioxide, is enriched in the gas phase during the deposition and then preferably condenses on the surface of the krypton grains thereby blocking the H_2 adsorption.

Adsorption phenomena on ionic oxides play a vital role in present surface research [17–20] and strong interaction between substrate and adsorbate is readily ascribed to point charges. In contrast to the ionic oxides a satisfying treatment of the solid carbon dioxide substrate and its mixtures by classical molecular dynamic simulation is possible and facilitates the interpretation of the experimental data. In this sense solid carbon dioxide is not only of intrinsic interest but appears to be a model oxide system. Its surface properties can be controlled by the amount of krypton added and monitored by the probe molecule H_2. The aim of the present inelastic neutron scattering (INS) study was to understand the surprisingly strong interaction between hydrogen molecules and the CO_2 surface.

Earlier studies allowed a profound understanding of the scattering of thermal neutrons from molecular hydrogen. The para-ortho conversion line $J = 0 \leftrightarrow 1$ can be observed directly and has a transition energy of ± 14.7 meV in the free molecule. The intensity ratio of the two lines on the neutron energy gain and loss sides, $(J = 1 \rightarrow 0)$ and $(J = 0 \rightarrow 1)$, respectively, reflects the para:ortho ratio of the hydrogen. In its condensed bulk phases [21] and isolated in Ar [22] or N_2 [23] H_2 exhibits rotational transitions at similar energies as in the free molecule. Even on catalytically active substances such as MoS_2 and WS_2 the $(J = 0 \rightarrow 1)$ line is broadened rather than shifted [24]. On surfaces of reactive oxides such as Al_2O_3 [18] and TiO_2 [19] the molecule sees strong anisotropic hindrance potentials which significantly shift the transition to lower energies [17]. The energy balance of the adsorption process shows that this redshift is equivalent to an enhanced adsorption enthalpy of ortho- with respect to para-hydrogen inducing an enrichment of the ortho species in the adsorbed phase.

The vibrational spectra of adsorbed hydrogen phases usually are quite different from the phonon density of states of bulk H_2 [24]. Depending on the surface structure the H_2 molecules can be adsorbed as isolated particles or as a two dimensional coherent layer. The vibrational dynamics of isolated adsorbed H_2 molecules are similar to those of light particles with the mass m isolated in a matrix of heavy molecules with mass M. Mannheim decomposed the dynamics of isolated particles into vibrations in resonance with the matrix and a local mode against it [25]. For $m/M < 0.5$, this is an Einstein mode with a frequency well above the phonon spectrum. In the case of surface adsorption resonant and localized modes describe the motion of the adsorbed species perpendicular to the surface. In a contiguous surface layer we expect additional phononlike vibrations parallel to the surface.

2 Experimental

The experiments were carried out at the time of flight-spectrometer IN4B in the Institut Laue-Langevin in Grenoble [26]. IN4B views a thermal neutron beam and employs a single graphite monochromator. By using first or second order of diffraction, incident energies of 17 and 68 meV, respectively, are provided. Data of groups of 36 detectors each were accumulated yielding a satisfying signal to noise ratio. Six spectra with average scattering angles in the range of $2\theta = 19^\circ$ to 100° were analyzed. Relative detector sensitivities and the instrumental resolution were calibrated using a vanadium sample. The energy resolution functions $f(E)$ were, to a good approximation, Gaussians with widths (fwhm) of 1 and 5 meV for 17 and 68 meV incident neutron energies, respectively.

All raw data were converted to scattering functions $S(\theta, E)$ given as a function of the Bragg angle θ and the energy transferred to the sample, $E = E_f - E_i$. E_i and E_f are the incident and final neutron energies, respectively. The hydrogen spectra were evaluated as differences of the data for charged and pure substrate and compared to calculated scattering functions $S_{cal}(\theta, E)$.

Gas mixtures (pure CO_2, 90:10 CO_2:Kr, 50:50 CO_2:Kr) were prepared by standard manometric procedures. The deposition rates were controlled by a mass flow controller (TYLAN FC260) to be 60 cm^3/min s.t.p. Hydrogen gas with a natural ortho:para ratio of 3:1 was employed in all experiments. The samples were prepared by gas phase deposition in an aluminium sample cell which was flanged to the end of a special insert [27] and cooled down to about 5 K in a liquid He-cryostat. The gas is introduced through a capillary which is insulated with respect to cold parts of the cryostat by a vacuum and heated by thermocoax wires to a temperature of 180 K during the deposition procedure permitting the codeposition of gases with very different triple point temperatures. Due to its insulation this capillary is not cooled down to the cryostat temperature but retains a temperature of approximately 50 K when switching off the heating after the deposition.

During the deposition some pressure of hydrogen built up on top of the sample, and the cell was pumped after the deposition. For the experiments with pure CO_2 and 90:10 CO_2:Kr substrates the pressure in the sample cell was low enough to avoid heating of the sample by thermal conduction to warmer parts. A small part of the sample was, however, exposed to thermal radiation of the gas outlet and had a temperature of about 20 K. The 50:50 CO_2:Kr substrate had a very low sorption capacity and a neutron signal of sufficient quality could only be obtained by admitting a hydrogen pressure of at least 0.1 mbar. By thermal conduction in this gas the total sample was heated to a temperature at which the solidification of H_2 was no more possible.

Our spectra unambiguously reflect the dynamics of hydrogen adsorbed on the CO_2 substrate. Estimates show that errors due to hydrogen in the gas phase or adsorbed elsewhere, or due to impurities in the sample cell are negligible, since the substrate surface area is very large: the mean area covered by a single hydrogen molecule is 11 $\mathring{A}^2$,

and a surface area of $83\,m^2$ is covered by a monolayer of $30\,cm^3$ s.t.p. of H_2. The area of the sample cell as exposed to the beam is only about 25 cm^2. Contributions to the scattering function by H_2 remaining in the gas phase or being condensed as liquid or solid can easily be distinguished from the spectra reported here by the rotational lines of the free molecule at 14.7 meV. We were not able to calculate the hydrogen coverage of the substrate from the preparation procedure, since its specific surface area is not known and strongly depends on the preparation conditions.

Large amounts of impurities could affect the data. Water in the CO_2 (L'Air Liquide, 99.99%) is below the detection limit of the experiment. Difficulties could arise if the hydrogen admitted to the sample would flush a large quantity of water from the gas handling system down to the substrate surface. This is very unlikely since the H_2 gas is admitted *via* a capillary being cooled to 180 K on a length of about 50 cm where water is rather frozen out than flushed away. Moreover the surface area of the sample handling system exposed to the hydrogen is small as compared to that of the substrate. Even the complete evaporation of several monolayers of water from the gas handling system could not poison a significant part of the CO_2-surface.

3 Theory

Theoretical scattering functions are calculated as a function of the modulus of the momentum transfer $\hbar Q$ and converted to $S_{cal}(\theta, E)$ using the relation:

$$\frac{(\hbar Q)^2}{2m_n} = E_i + E_f - \sqrt{2E_iE_f\cos\theta} \tag{1}$$

where m_n is the neutron mass. $S_{cal}(\theta, E)$ accounts for vibrations ($S_{vib}(\theta, E)$) and rotations ($S_{rot}(\theta, E)$) of hydrogen bound to definite surface sites, as well as for diffusion ($S_{diff}(\theta, E)$) in a two dimensional liquid. In this section we develop the analytical form of these components. The physical background of this formulation is given in the discussion.

$S_{rot}(\theta, E)$ is introduced into the calculation as a line spectrum. The experimental energy window contains six transitions: $J \to J'$: $0 \to 0$, $1 \to 1$, $0 \leftrightarrow 1$, $1 \to 2$, and $0 \to 2$. Position and intrinsic width of $J \to J'$: $1 \to 0$ are directly evaluated from the line observed in the energy gain part of the spectra in Figures 2a, b. The relative intensities of the rotational transitions are determined by Q dependent formfactors, which include the coherent and incoherent scattering cross sections of H. We approximated the intensities of the rotational transitions observed here by the formfactors of the free rotations given in [28], although the line shift in principle is related to a modification of the rotational wave functions and thus of the formfactors [17]. According to the Young-Koppel model the intensity of para-para transitions such as $J \to J'$: $0 \to 0$ and $0 \to 2$ is governed by the small coherent neutron scattering cross section of hydrogen and thus may be neglected here.

The centre-of-gravity hydrogen vibrations are described by an empirical phonon density of states $Z(E)$ (Fig. 4a), which is composed of a small number of Gaussians. This allows the phonon spectrum to be adapted to the experimental data by the variation of only a few parameters. This phonon density can represent dispersed two-dimensional modes of hydrogen layers as well as Einstein modes of decoupled molecules. It was shown in [25,29–31], that Einstein modes can be included into $Z(E)$.

The interactions of H_2 molecules with other atoms or molecules are in general weak. In spite of the low mass the phonon frequencies are only of the order of a few meV [21,22,32]. Consequently the zero point mean-squared displacement of motion u^2 is as high as 0.46 Å^2 [32], and thermal neutron spectra contain strong combination modes [33]. At epithermal energies the spectrum of molecular hydrogen is very well described by the impulse approximation [34]. In the intermediate Q-range where multiphonon transitions have already to be taken into account but the impulse approximation does not yet apply, the calculation of the scattering function from the phonon density of states in principle is tedious since a sum of convolution products of the phonon density of states has to be evaluated [35]. In [30,36] a simple algorithm has been introduced, which does not make recurrence to the multiphonon expansion ([37], Eqs. (4.68, 4.69)), but describes the scattering function of a harmonic oscillator in a closed form. We rewrite equation 4.239 of [37]:

$$\begin{aligned} S(Q,E) &= \frac{\sigma}{8\pi^2\hbar}\int_{-\infty}^{\infty} dt \exp\left(-\frac{iEt}{\hbar}\right) \\ &\quad \times \exp\left(\frac{\hbar Q^2}{2M}[\gamma(t)-\gamma(0)]\right) \\ \gamma(t) &= \int_{-\infty}^{\infty}\frac{Z(E)dE}{E} n_B(E)\exp\left(\frac{iEt}{\hbar}\right) \\ \frac{\hbar^2Q^2}{2M}\gamma(0) &= \frac{\hbar^2Q^2}{2M}\int_{-\infty}^{\infty}\frac{Z(E)dE}{E} n_B(E) = 2W(Q) \\ n_B(E) &= \frac{1}{\exp\left(\frac{E}{kT}\right)-1} \end{aligned} \tag{2}$$

as

$$\begin{aligned} S(Q,E) &= \frac{\sigma}{8\pi^2\hbar}\exp(-2W(Q))\int_{-\infty}^{\infty} dt \exp\left(-\frac{iEt}{\hbar}\right) \\ &\quad \times \exp\left(\frac{\hbar Q^2}{2M}\int_{-\infty}^{\infty}\frac{Z(E)dE}{E} n_B(E)\exp\left(\frac{iEt}{\hbar}\right)\right) \end{aligned} \tag{3}$$

where $n_B(E)$ is the Bose factor. This reformulation can be evaluated straightforwardly for any $Z(E)$ and allows the contributions of elastic as well as single and multiphonon scattering of infinite order to be treated in closed form.

The quasielastic scattering function $S_{diff}(Q, E)$ for diffusing molecules was taken from [38]:

$$S_{diff}(Q,E) = \frac{DQ^2}{(DQ^2)^2+E^2}\cdot\frac{E}{1-\exp\left(\frac{E}{k_BT}\right)} \tag{4}$$

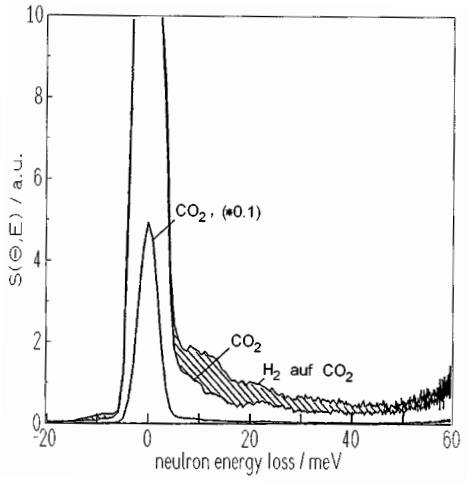

Fig. 1. Inelastic neutron scattering spectra of vapour deposited CO_2 with (upper line) and without adsorbed hydrogen, recorded with an incident energy of 68 meV.

D, k_B and T are the diffusion coefficient, the Boltzmann constant and the temperature, respectively. The first factor on the right hand side is a Lorentzian which describes the quasielastic scattering caused by the translational diffusion of hydrogen molecules. As large energy transfers have been employed at a temperature of only 20 K, a detailed balance correction is afforded, which is given by the second factor [38].

Below we will introduce a model for the H_2-adsorption which provides a solid phase of molecules which undergo hindered rotation and well defined vibrational motions and a second phase with liquidlike diffusion. In the frame of this model the total scattering function $S_{cal}(\theta, E)$ is given by:

$$S_{cal}(\theta, E) = (N_{com} S_{rot}(\theta, E) \otimes S_{vib}(\theta, E) + N_{inc} S_{diff}(\theta, E)) \otimes f(E) \quad (5)$$

where $\otimes$ denotes a convolution product and N_{com}, N_{inc} are normalisation factors describing the relative intensities of the commensurate and of the incommensurate phase, respectively.

4 Results

In a first experiment a mixture of 5.4 l s.t.p. CO_2 with 1.5 mol% of hydrogen was deposited at 5 K yielding an intense spectrum. By heating the sample to 70 K the hydrogen was removed, and after cooling down again to 5 K, the reference spectrum of pure CO_2 was obtained (Fig. 1). In the energy loss range the intensity due to the hydrogen is similar to that from the phonons of the CO_2 substrate. In the energy gain part all inelastic intensity beyond the tail of the instrumental resolution function disappears when pumping off the H_2. Then the sample was recharged with hydrogen and a third spectrum was recorded. We achieved an adsorption of 30 cm^3 s.t.p. H_2 being sufficient to yield another intense hydrogen spectrum. A comparison between the two resulting difference spectra from codeposited and from adsorbed hydrogen showed no significant discrepancies, apart from the smaller intensity of the latter one. All further samples were prepared by first depositing the substrate and then charging it with hydrogen.

Figures 2 and 3 show the spectra of hydrogen after subtraction of the data from the respective unloaded substrates for 17 meV and 68 meV neutron incident energies, respectively. In each spectrum on pure CO_2 (Fig. 2a) we find a well defined peak at -9.4 meV in the energy gain region, which is slightly broader than the elastic line. In the energy gain range the instrument resolution function is broadened with respect to the elastic line since the neutron time of flight from sample to detector is smaller and the respective measuring error increases. Therefore, we attribute the width of the inelastic peak to the instrument resolution rather than to intrinsic broadening. In spectra of the same sample at 68 meV incident energy this line is reduced to a wing of the elastic peak (Fig. 3) due to the lower instrumental resolution. We assign this excitation to the ortho-para transition $J \to J'$: $1 \to 0$ which is considerably shifted from -14.7 meV in the free molecule to -9.4 meV in the adsorbed one.

In a further experiment hydrogen was adsorbed on the surface of a vapour deposited mixture of 90:10 CO_2:krypton. The adsorption ability of the substrate experiences a strong decrease even with only 10 mol% of krypton, but no qualitative change with respect to the pure CO_2 substrate (Fig. 2a) is observed in the spectrum (Fig. 2b). The ortho-para conversion line is well reproduced at -9.4 meV, but now has an intrinsic width of 0.8 meV.

The appearance of a strong inelastic feature in neutron energy gain spectra is unexpected for cold samples. The transition energy $E = 9.4$ meV corresponds to $E/k_B = 115$ K ($k_B = 81.7\,\mu$eV/K) which is much higher than the physical temperature. Time-of-flight spectrometers may, under unfavourable conditions, yield parasitic features in the inelastic spectra. We rule out this possibility for the line at -9.4 meV since (i) the substrate spectra do not show inelastic features in energy gain, (ii) the position of the line does not depend on the scattering angle even in the well resolved spectra with 17 meV incident energy, (iii) the feature also occurs with 68 meV incident energy, and (iv) the spectra of H_2 on pure CO_2 and of H_2 on 90:10 CO_2:Kr were obtained in two independent experiments.

On the neutron energy loss side no feature corresponding to the line at -9.4 meV is found. We rather see a broad intensity distribution starting near the elastic line. Its width increases with increasing Q and its maximum shifts to higher energy transfers. It eventually extends to the limit of the neutron incident energy. Other than on the energy gain side the spectra from the substrate alone show a high intensity on the energy loss side, which is due to the lattice phonons of pure CO_2 (Fig. 1). Thus the difference spectra of the adsorbed hydrogen have a smaller signal/noise ratio in this energy range. We compensated

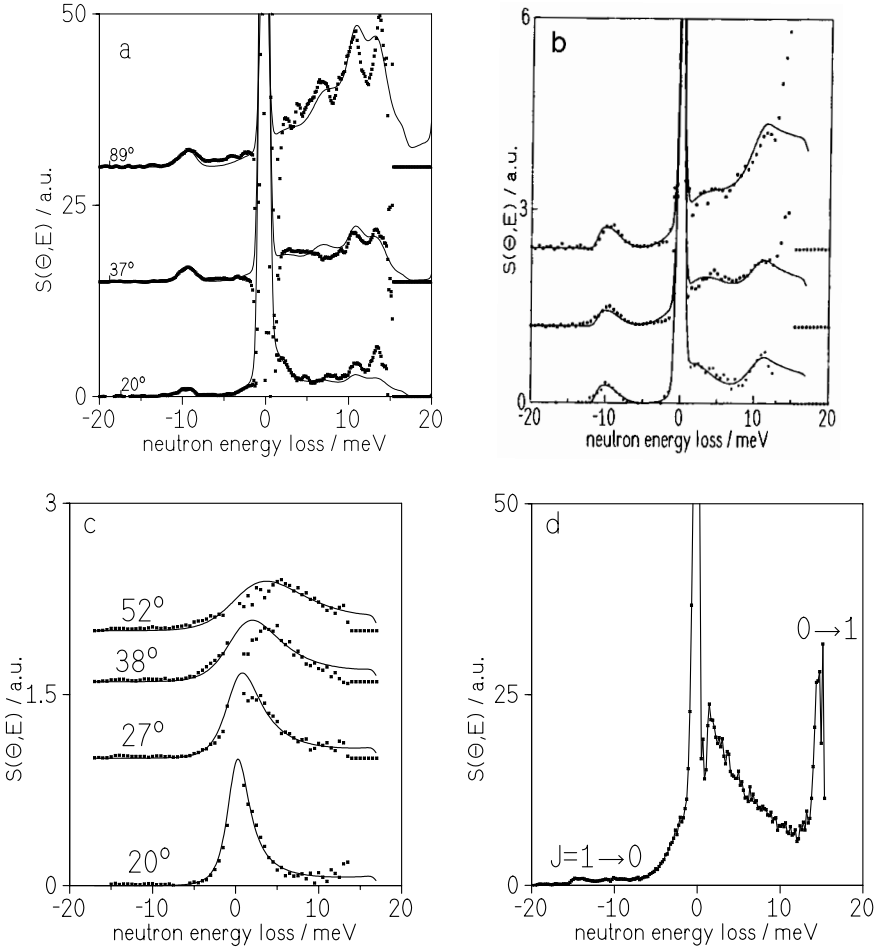

Fig. 2. Inelastic neutron scattering spectra of adsorbed hydrogen, recorded with an incident energy of 17 meV (symbols) and fits by calculated scattering functions (full curves). The corresponding scattering angles are indicated in the figure. a) on pure CO_2 substrate, b) on 90:10 CO_2:Kr, c) on 50:50 CO_2:Kr, H_2 pressure = 0.1 mbar, d) on 50:50 CO_2:Kr, H_2 pressure = 10 mbar, sum over all angles (symbols and full line represent the data).

for this shortcoming by recording data with two incident energies in a wide range of energy and momentum transfers thus obtaining a very well defined scattering function. The overall shape of the spectra (Figs. 2a, 3) changes very significantly as a function of the momentum transfer.

Spectra of H_2 on 50:50 CO_2:Kr were recorded with two different hydrogen pressures in the sample corresponding to different coverages. At pressures around 0.1 mbar, neither rotational transitions nor significant phonon excitations were observed (Fig. 2c). The spectra of hydrogen on this substrate show the typical shape and Q-dependence as expected for quasielastic scattering. It could be fitted by the quasielastic scattering function $S_{diff}(Q, E)$ given in equation (4). This fit describes translational diffusion, with the diffusion constant D being the only fit parameter apart from overall normalization. The best fit is obtained for $D = 4.4 \times 10^{-5}\,\mathrm{cm}^2/\mathrm{s}$. In contrast to the spectra of bulk liquid H_2 clearly no rotational transitions have been found here, however. At pressures around 10 mbar additional features were observed (Fig. 2d). On the energy loss side most likely the para-ortho transition appears at

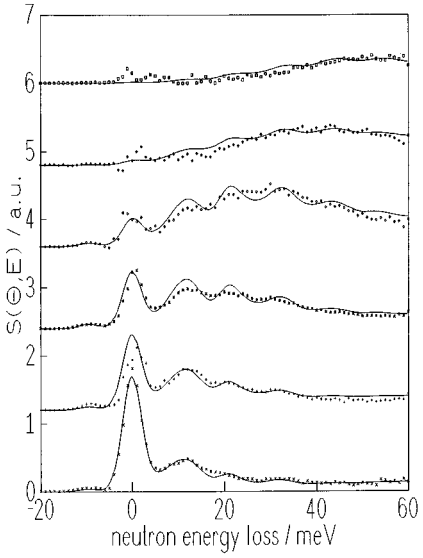

Fig. 3. Spectra of hydrogen on pure CO_2 recorded with 68 meV incident energy, and corresponding fits.

14.7 meV being not significantly shifted with respect to bulk H_2 whereas a broad feature is seen in energy gain extending from −14.7 meV to the onset of the quasielastic intensity.

The fit of the spectra from H_2 on pure CO_2 as well as on 90:10 CO_2:Kr $S_{diff}(Q,E)$ significantly improves when adding a small contribution of quasielastic scattering (Figs. 2a, 2b, 3). Especially at low scattering angles the elastic line has wings which cannot be fitted by equation (3). $S_{diff}(Q,E)$ in these spectra was calculated with the value for D as found for H_2 on 50:50 CO_2:Kr (Fig. 2c).

5 Discussion

The INS-spectra give information about the dynamics of the adsorbed hydrogen. We assign the two scattering functions for rotation and phonons, and for translational diffusion, respectively, to two different adsorbed phases of the molecular H_2. We will discuss the origin of the downshift of the $J = 1 \rightarrow 0$ transition and relate it to the properties of the substrate, further discuss the fit of the phonon spectra and finally the quasielastic data.

The general model for the downshift of rotational lines provides an anisotropic potential which imposes energetic barriers to the rotation and transfers it to rotational tunnelling [17]. In the frame of this approach, a shift of the ortho-para conversion line from −14.7 to −9.4 meV corresponds to an energy barrier of the order of 20 meV. Figure 5 shows a simplified point charge model for the interaction of a single adsorbed H_2 molecule with a single CO_2 substrate molecule at a mutual distance of 3.8 Å. The charges on the C, O, and H atoms, as well as in the centre of the H_2 molecule are chosen as to reproduce the experimental quadrupolar moments. The parallel and the twisted configurations have strongly attractive Coulomb interaction energies (−60 and −80 meV, respectively). These values are similar to the measured adsorption enthalpy (65 meV, [11]). The difference of the two interaction energies, 20 meV, correlates with the barrier for rotation. The third orientation of the H_2 molecule perpendicular to the CO_2 is extremely unfavourable, since the quadrupole moments of the two molecules have opposite signs.

Another approach relates the observed shift of the ortho-para transition to the different multipole moments of ortho- and para-H_2. In two adjacent ortho-H_2 molecules the $J = 1$ state which is triply degenerate in the free molecule splits into three levels, which are separated from each other by intervals of about 0.75 meV [15]. This interaction leads to orientational order in low temperature o-H_2 crystals. The modulus of the quadrupole moment of CO_2 is about seven times higher than that of ortho-H_2 most likely inducing a much stronger splitting of the $J = 1$ level in an adjacent ortho-H_2. We may thus attribute the observed shift of 5.3 meV to the quadrupole-quadrupole interaction of o-H_2 with the CO_2. The adsorbed ortho-H_2 will be nearly completely in the lowest of the states resulting from the $J = 1$ level in the free molecule since the shift is higher than k_BT. Therefore, only one ortho-para transition is observed in the spectra.

It has to be discussed why the line at −9.4 meV (Figs. 2a, 2b, 3) is seen with considerable intensity but no corresponding signal on the energy loss side. In neutron scattering experiments on condensed natural hydrogen the ortho-para line is observed [22] since the spin forbidden conversion of ortho to para-H_2 is slow as compared to the timescale of data acquisition [15]. On the other hand the para-ortho line is weak, smeared out and superposed on a high background. At the low temperatures employed the ortho-H_2 is preferentially adsorbed on the CO_2 surface, since its quadrupole-quadrupole interaction with CO_2 adds to the adsorption energy. This effect is well known and has been used for the separation of the ortho- and para modifications [17]. The difference in the adsorption enthalpies of ortho-H_2 and para-H_2 is identical to the downshift of the $J = 0 \rightarrow 1$ line which amounts here to 5.3 meV. Possibly during deposition mainly ortho-hydrogen was adsorbed, whereas the para-H_2 was pumped off afterwards.

The remaining intensity of the $J = 0 \rightarrow 1$ transition may be smeared out over a large energy range due to the splitting of the $J = 1$ level, since all $J = 1$ states contribute to the para-ortho transition resulting in a broadening. In contrast to that the sharp ortho-para transition sits on a small background, since at low temperatures no phonon transitions are observed in the energy gain spectrum. Phonons of hydrogen are, however, the predominant contribution to the energy loss part of the spectra (Figs. 2a, 2b).

Whereas the assignment of the peak at −9.4 meV is straightforward and the downshift of a rotational line in an external potential is a well known effect, the correlation of this hindrance potential to the surface properties is somewhat more speculative.

We observed earlier [2,5,8] that carbon dioxide even under conditions of rapid gas phase deposition forms well defined crystalline lattices. Vapour deposition of carbon dioxide induces a high nucleation rate which results in very small grains with a high specific surface area, but no significant intrinsic disorder. The structure of the adsorption sites depends on the crystallographic indices of the most stable CO_2 surface, which is not known to us. Our electrostatic model only takes into account the interaction between single H_2 and CO_2 molecules and therefore does not reproduce the influence of the surface structure at all. It is obvious, however, that further CO_2-molecules will contribute to some extent to the potential experienced by an adsorbed H_2-molecule. By the introduction of 10% Kr, *e.g.*, the ortho-para transition is broadened. This may be attributed to the reduction of the orientational order of the surface by Kr [1].

It has further to be discussed, why hydrogen yields the same spectra when codeposited with CO_2 and when adsorbed on the surface after the deposition, apart of the absolute intensity. H_2 trapped in substrate cages should yield different spectra than adsorbed on the surface. Since the two gases have very different vapour pressures at the deposition temperature, it is likely that H_2 and CO_2 never condensed at the same time trapping the hydrogen in CO_2

cages, but that H_2 enriched in the vapour phase on top of the condensing CO_2. Only after solid CO_2 was formed H_2 adsorbed on its surface. During evaporation of the codeposited hydrogen sintering of the carbon dioxide grains occurred reducing the surface area. Therefore, after evaporation of the codeposited hydrogen only a smaller amount could be adsorbed again yielding weaker spectra.

The hydrogen coverage of the surface cannot be determined directly since the specific surface area of the solid CO_2 depends on its preparation and is not known. Based on our interpretation of the line at −9.4 meV it seems to be likely, that the data plotted in Figures 2a, 2b and Figure 3 correspond to monolayer or even sub-monolayer coverage, whereas Figure 2d reflects multilayer adsorption. When depositing an increasing number of H_2 layers, the condensate will finally attain bulk hydrogen properties and show the line of nearly free rotation at −14.7 meV. The shift of this line to −9.4 meV reflects a strong external hindrance potential which is obviously due to the CO_2 surface. Going from the surface layer into higher adsorbed layers there will be a gradual reduction of line shift since the contribution of the CO_2 substrate to the hindrance potential will be consecutively screened by the bottom layers. In higher adsorption layers we expect intermediate line positions between −9.4 meV and −14.7 meV, as is observed at higher hydrogen pressures favouring multilayer adsorption (Fig. 2d).

On the other hand the sharp line at −9.4 meV (Figs. 2a, 2b) reflects a strong anisotropic hindrance potential which is nearly constant for all adsorbed hydrogen molecules. According to our electrostatic model, the hindrance potential depends sensitively on the distance between adsorbed molecule and surface CO_2 molecule. It is, therefore, unlikely that the rotation of H_2 in the second and higher adsorption layers experiences the same line shift as in the lowest layer. This indicates monolayer or sub-monolayer adsorption for the spectra in Figures 2a, 2b.

A further question is why the hindrance potential in the monolayer is constant at all. In general it depends on the positions of the H_2 molecules relative to the surface CO_2 molecules. By thermodynamic reasons H_2 adsorption will first take place at sites with a local energy minimum. In case of a regular substrate structure there will be many sites with nearly identical structure and hindrance potentials. We speculate that this leads to a commensurate adsorption, being favoured by the similarity of the hard sphere diameters of CO_2 and H_2 in their respective crystals (4.1 [39] and 3.8 Å [40]).

For calculating $S_{vib}(\theta, E)$ a phonon density of states $Z(E)$ for the intermolecular vibrations of the adsorbed molecular hydrogen was generated here (Fig. 4a). The best fit was obtained assuming two features at energies below 18 meV and around 32 meV. The ratio of the integrated intensities of the low and high frequency parts is 2:1. The low frequency part of $Z(E)$ was set up to be similar to the bulk phonon density of states of solid CO_2 (Fig. 4c, data from [41]). This implies that modes of the H_2 molecules in resonance with the bulk CO_2 are observed. In addition

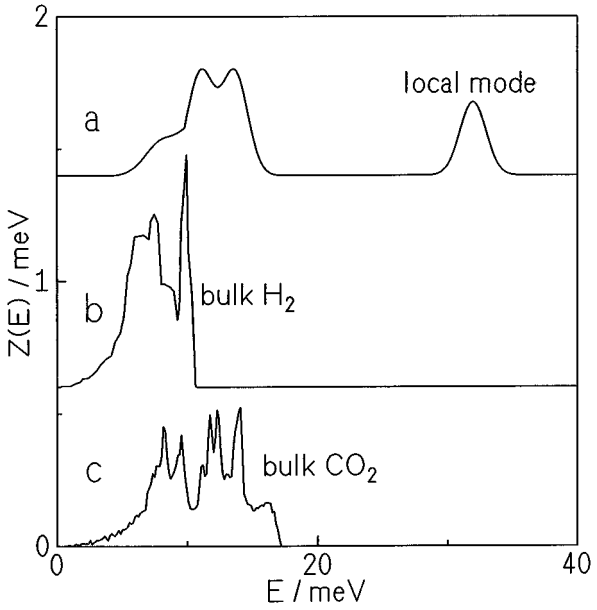

Fig. 4. Phonon densities of states a) as used for fit of the spectra in Figures 1a, 2, b) of pure H_2, from [21], c) of pure CO_2, from [41].

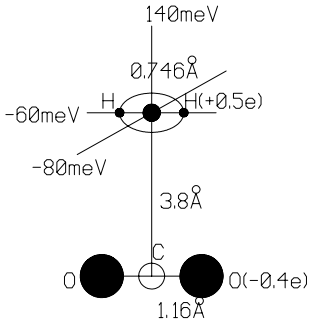

Fig. 5. Point charge model for the electrostatic interaction of an adsorbed H_2 molecule with one surface CO_2. H_2 is represented by two positive charges at the proton positions and a negative charge in the centre, CO_2 by point charges at its atom positions. The charges are given in the figure as fractions of the electron charge, they reproduce the quadrupole moments of the two molecules. For the three orientations of the H_2 molecule Coulomb interaction energies of −60, −80 and 140 meV are found.

to that a two dimensional phononlike motion may occur in the H_2-monolayer. This is accounted for in $Z(E)$ of Figure 4a by an additional intensity in the range of bulk hydrogen phonons (Fig. 4b, data from [21]). As the mass of H_2 is smaller than half the CO_2 mass, in addition to the resonant modes a local Einstein mode above the range of dispersed lattice modes will occur [25]. The exact position, relative intensity and intrinsic width of this local mode in $Z(E)$ were refined as free parameters. The energy of 32 meV as found here is well below the adsorption enthalpy of 65 meV [11].

This $Z(E)$ allowed spectra to be fitted in the full range of momentum and energy transfers (Figs. 2a, 2b, 3) according to equations (1–4). In the spectra taken with an incident energy of 17 meV (Fig. 2) mainly single phonon transitions are seen. With increasing Q, the spectrum continuously shifts to higher energies, since multiphonon transitions appear. This holds especially for data recorded with an incident energy of 68 meV below $2\theta = 40°$. At the highest scattering angles the shape of the scattering function is well described by the impulse approximation with a kinetic energy of 115 K for the centre-of-mass dynamics of H_2. This energy is significantly higher than in bulk solid H_2 (76 K [24,34]) since the phonon spectrum of the adsorbed H_2 is shifted to higher energies due to the Einstein mode (Fig. 4). A similar observation was reported in [24]. For appreciating the quality of the fit it has to be taken into account that not only each spectrum in Figures 2 and 3 is fitted by the calculation nearly within the experimental error limits but that the fitting of spectra in a large Q-range which look completely different as a function of energy transfer was achieved by one common set of parameters.

There remain slight discrepancies between measured and calculated data, since some ripples in the energy loss spectra in Figure 2 are not fully reproduced by the calculation. In Figure 3 the calculation yields a slightly more pronounced structure than is found in the measured data. We ascribe this disagreement to our $Z(E)$. It has been shown in earliler work on local and resonant modes of matrix isolated molecules [25], that the local density of states which describes the resonant modes of the isolated molecule is in general not identical to the phonon density of states of the substrate. We did not take into account this effect since this would have implied the use of further unknown parameters such as force constants. Our $Z(E)$ as generated by a few number of Gaussians only affords a small number of parameters.

The quasielastic scattering function was observed for 50:50 CO_2:Kr substrates and as a minor contribution also in the other spectra. It is assigned to translational diffusion of the hydrogen molecules. On warmer parts of the substrate they form a liquid film. The diffusion coefficient reported here ($D = 4.4 \times 10^{-5}\,\mathrm{cm}^2/\mathrm{s}$) is equal to the value found for bulk liquid hydrogen at 15 K [42]. In our experiment the temperature was slightly higher corresponding to a higher bulk diffusion constant. On the other hand barriers in the surface may slow down the diffusion in the adsorbate.

This scattering function does not contain rotational transitions as are observed in bulk liquid H_2 [43]. A possible explanation for that is that the height and symmetry of the hindering potential that influences the molecule rotation depends on the momentary position of the diffusing molecules. This leads to broad, smeared-out rotational transitions which could not be identified in the spectra (Fig. 2c).

6 Conclusions

The understanding of interactions of carbon dioxide with other molecules is of great interest for applications such as extraction by CO_2 fluids. Since its neutron spectra are relatively simple hydrogen is well suited as a probe molecule. It is shown here that neutron spectra yield sufficient information for developing a fairly detailed model of the adsorption process, which in turn allows to understand the intermolecular interactions present.

The adsorption of hydrogen on solid carbon dioxide induces an unexpectedly strong redshift of the $J = 1 \rightarrow 0$ transition, which was so far only found on ionic oxides. We could explain semi-quantitatively the shift by the quadrupole-quadrupole interaction between carbondioxide and ortho-H_2 and reproduce the corresponding interaction strength by a simple point charge model. The simplest scenario for the adsorption provides a commensurate monolayer at low hydrogen pressures, whereas at higher pressures a multilayer system builds up which gradually attains the properties of the bulk solid. Quasielastic scattering allows liquidlike film to be detected at higher temperatures.

With the scattering function $S_{cal}(Q, E)$ described so far we were able to fit all measured spectra of H_2 on pure CO_2 with one common set of parameters. The agreement is very satisfying since there are severe constraints imposed on this fit. It has to be based on a sensible physical model for the dynamics of the adsorbed molecules, and must reproduce the drastic variation of the experimental data from single phonon spectra to multiphonon and impulse approximation regime in the wide range of momentum transfers applied.

We thank Drs. H.-W. Fleger and P. Beichert for assistance during the neutron scattering experiments. W.L. gratefully acknowledges a Heisenberg fellowship. This work has been funded by the German Federal Minister for Research and Technology (BMFT) under the contract numbers 03 KN2 SIE and 03 KN3 SIE and by the Fond der Chemischen Industrie (E.K. and W.L.).

References

1. W. Langel, H.-W. Fleger, E. Knözinger, Ber. Bunsenges. Phys. Chem. **98**, 81 (1994).
2. E. Knözinger, W. Schuller, W. Langel, J. Phys. Chem. **97**, 927 (1993).
3. F.L. Whipple, W.F. Huebner, Ann. Rev. Astron. Astrophys. **14**, 143 (1976).
4. G. Brunner, *Gas Extraction* (Darmstadt, 1994).
5. H.-W. Fleger, W. Langel, E. Knözinger, W. Schuller, Ber. Bunsenges. Phys. Chem. **99**, 940 (1995).
6. W. Langel, W. Schuller, E. Knözinger, H.-W. Fleger, H.J. Lauter, J. Chem. Phys. **89**, 1741 (1988).
7. W. Langel, M. Prager, H.-W. Fleger, E. Knözinger, H.-J. Lauter, H. Blank, C. Carlile, J. Chem. Phys. **98**, 4838 (1993).

8. H.-W. Fleger, *Modelle und Molekulardynamische Simulation zur Fehlordnung in gasphasendeponierten Ar^-, CO_2^- und CO_2/Kr-Festkörpern* (Aachen: Shaker, 1992).
9. A.D. Buckingham, R.L. Disch, Proc. Roy. Soc. **A273**, 275 (1963).
10. G. Cardini, V. Schettino, M. Klein, J. Chem. Phys. **90**, 4441 (1989).
11. W. Schulze, H. Abe, Chem. Phys. **52**, 381 (1980).
12. V.B. Yuserov, F.I. Busol, Sov. Phys. Techn. Phys. **11**, 1518 (1967).
13. V.B. Yuserov, R.F. Bulatova, P.M. Kobzev, V.S. Kosan, Sov. Phys. Techn. Phys. **13**, 238 (1968).
14. V.B. Yuserov, P.M. Kobzev, Sov. Phys. Techn. Phys. **14**, 1261 (1970).
15. I.F. Silvera, Rev. Mod. Phys. **52**, 393 (1980).
16. A. Mews, Thesis (Siegen, 1993).
17. D. White, E.N. Lassettre, J. Chem. Phys. **32**, 72 (1960).
18. I.F. Silvera, M. Nielsen, Phys. Rev. Lett. **37**, 1275 (1976).
19. R.K. Thomas, in *Quantum Aspects of Molecular Motions in Solids*, edited by A. Heidemann, A. Magerl, M. Prager, D. Richter, T. Springer (Berlin, Heidelberg, New York: Springer, 1987).
20. A. Knipp, *Inelastische Neutronenstreuung an physisorbiertem Wasserstoff auf hochdispersen Oxiden* (Aachen: Shaker, 1993).
21. A. Bickermann, *Inkohärente Neutronenstreuung an festem Wasserstoff*, Report of Kernforschungsanlage Jülich Nr. 1487 (1978).
22. W. Langel, Rev. Phys. Appl. **19**, 755 (1984).
23. F.T. Prochaska, L. Andrews, J. Chem. Phys. **32**, 72 (1960).
24. P.N. Jones, E. Knözinger, W. Langel, R.B. Moyes, J. Tomkinson, Surf. Sci. **207**, 159 (1988).
25. P.D. Mannheim, Phys. Rev. B **5**, 745 (1972).
26. Guide to Neutron Scattering Facilities at the ILL (Grenoble: Institut Max von Laue-Paul Langevin, 1988).
27. W. Langel, H. Kollhoff, E. Knözinger, J. Phys. E: Sci. Instrum. **19**, 86 (1986).
28. J.A. Young, J.U. Koppel, Phys. Rev. A **135**, 603 (1964).
29. M. Warner, S.W. Lovesey, J. Smith, Z. Phys. B **56**, 13 (1984).
30. W. Langel, *Mikrostruktur inhomogener Festkörper*. Siegen, 1989.
31. W. Langel, Spectrochimica Acta **48A**, 405 (1992).
32. M. Nielsen, Phys. Rev. B **7**, 1626 (1972).
33. W. Langel, J. Mol. Struct. **143**, 1 (1986).
34. W. Langel, D.L. Price, R.O. Simmons, P. Sokol, Phys. Rev. B **38**, 11275 (1988).
35. A. Sjölander, Ark. Fys. **14**, 315 (1958).
36. J. Mayers, C. Andreani, G. Baciocco, Phys. Rev. B **39**, 2022 (1989).
37. S.W. Lovesey, *Theory of Neutron Scattering from Condensed Matter*. (Oxford: Oxford University Press, 1987).
38. S. Grondey, M. Prager, W. Press, A. Heidemann, J. Chem. Phys. **85**, 2204 (1986).
39. I.N. Krupskil, A.I. Prokhvatilov, A.L. Erenburg, A.S. Barylnin, Sov. J. Low Temp. Phys. **8**, 263 (1982).
40. R.L. Mills, A.F. Schuch, Phys. Rev. Lett. **15**, 722 (1965).
41. G. Cardini, P. Procacci, R. Righini, Chem. Phys. **117**, 355 (1987).
42. D.E. O'Reilly, E.M. Peterson, J. Chem. Phys. **66**, 934 (1977).
43. P.A. Egelstaff, B.C. Haywood, F.J. Webb, Proc. Phys. Soc. **90**, 681 (1967).